J. Fluid Mech. (2010), *vol.* 661, *pp.* 316–340. © Cambridge University Press 2010
doi:10.1017/S0022112010002983

Beach-face evolution in the swash zone

DAVID MATTHEW KELLY† AND NICK DODD

Environmental Fluid Mechanics Research Centre, Process and Environmental Division, Faculty of Engineering, University of Nottingham, University Park, Nottingham NG7 2RD, UK

(Received 13 August 2009; revised 24 May 2010; accepted 26 May 2010; first published online 2 August 2010)

We investigate swash on an erodible beach using the one-dimensional shallow-water equations fully coupled to a bed-evolution (Exner) equation. In particular, the dam-break/bore-collapse initial condition of Shen & Meyer (*J. Fluid Mech.*, vol. 16, 1963, pp. 113–125) and Peregrine & Williams (*J. Fluid Mech.*, vol. 440, 2001, pp. 391–399) is investigated using a numerical model based on the method of characteristics. A sediment-transport formula (cubic in velocity u: Au^3) is used here; this belongs to a family of sediment-transport formulae for which Pritchard & Hogg (*Coastal Engng*, vol. 52, 2005, pp. 1–23) showed that net sediment transport under the Shen & Meyer (1963) bore collapse is offshore throughout the swash zone when a non-erodible bed is considered. It is found that full coupling with the beach, although still resulting in the net offshore transport of sediment throughout the swash zone, leads to a large reduction in the net offshore transport of sediment from the beach face. This is particularly true for the upper third of the swash zone. Moreover, in contradistinction to swash flows over non-erodible beds, flows over erodible beaches are unique to the bed mobility and porosity under consideration; this has very important implications for run-up predictions. The conclusion is that it is essential to consider full coupling of water and bed motions (i.e. full morphodynamics) in order to understand and predict sediment transport in the swash, regardless of other physical effects (e.g. turbulence, infiltration, pre-suspended sediment, etc.).

Key words: coastal engineering, sediment transport, shallow-water flows

1. Introduction

The swash zone is the flow region that is successively covered and uncovered by the run-up and backwash of water as waves impinge on a beach. This zone is, in some ways, the most dynamic region of the nearshore; here, flow velocities are high ($>2\,\mathrm{m\,s^{-1}}$) and water depths close to the leading edge or shoreline are very small. Due to these high flow velocities, the swash zone is characterized by a rapid morphological change (Masselink & Puleo 2006). Water motion in the swash zone of steeper beaches is typically driven by the turbulent bores that result from waves breaking near or at the shore. There are also instances when waves do not break but instead surge up and down the beach (see Carrier & Greenspan 1958). Principal variables affecting wave breaking are wave period, wave height and beach slope. These variables can be combined to give the (dimensionless) surf similarity parameter, which describes if and how waves break (see, e.g., Mei 1990). However, on most beaches, waves do break and it is for this reason that hereafter this paper focuses solely on bore-driven swash.

† Email address for correspondence: evxdmk@nottingham.ac.uk

https://doi.org/10.1017/S0022112010002983 Published online by Cambridge University Press

Present theoretical understanding of bore-driven swash is primarily down to the work of Whitham, Meyer, Peregrine and co-workers (Whitham 1958; Keller, Levine & Whitham 1960; Ho & Meyer 1962; Shen & Meyer 1963; Hibberd & Peregrine 1979; Barker & Whitham 1980; Packwood & Peregrine 1980). Whitham (1958) was the first to show that, within the framework of the shallow-water theory, bore height must tend to zero as the original shoreline position is approached while the bore velocity tends to some limiting value $\hat{U}_b$. Despite the fact that, in reality, this process occurs over finite time and length scales, several investigators (e.g. Freeman & Le Méhauté 1964, Barker & Whitham 1980 and Guard & Baldock 2007) have noted that the problem of bore collapse can effectively be reduced to that of a dam-break on a slope. Furthermore, Peregrine & Williams (2001) have shown that a specific dam-break initial-value problem actually produces swash identical to that described by the analytical solution of Shen & Meyer (1963), hereafter referred to as SM63. Although the SM63 solution was derived using a generic seaward boundary condition, and thus, does not necessarily correspond to any physically realistic offshore conditions (see § 3.1 for more on this), the knowledge of the corresponding initial conditions and the lack of any other explicit analytical solution motivate its use here. It is worth noting that Pritchard, Guard & Baldock (2008) have recently provided a more general implicit analytical solution for bore-driven swash. Within the last 10 years, cross-shore sediment transport within the swash zone has become a topic of major interest, primarily because of its role in determining beach morphology and shoreline position. This interest has generated a number of numerical (e.g. Masselink & Li 2001) and field studies (e.g. Butt *et al.* 2004). The net transport of sediment over a single swash event tends to be a small difference between two large quantities (Osborne & Rooker 1999), and it is recognized that there are many interrelated factors that determine the amount of sediment transport within the swash zone (Masselink & Hughes 1998). The majority of numerical studies utilize a sediment-transport formula to express sediment flux and this is deemed a function of either one or both shallow-water hydrodynamic variables (depth and depth-averaged velocity). In a recent paper, Pritchard & Hogg (2005) (hereafter referred to as PH05) have shown that, due to the inherent asymmetry of the flow field, all swash models that use power-law-based sediment-transport formulae in which the hydro- and morphodynamics are decoupled predict net offshore transport of sediment everywhere on the beach. PH05 noted that this was at odds with the findings of field studies (see Masselink *et al.* 2005), which indicate that, under certain conditions, single swash events can produce a net onshore movement of sediment. In order to resolve this discrepancy between model predictions and field data, PH05 developed an uncoupled analytical model that included terms for pre-suspended sediment and settling lag. The inclusion of these terms led to the possibility of local net onshore transport of sediment. Interestingly, the critical factor was found to be the amount of sediment brought into suspension at initial bore collapse rather than settling lag time.

In this paper, we employ a mathematical model in which the hydro- and morphodynamics are coupled directly such that the bed and flow interact fully within the constraints imposed by the inviscid shallow-water dynamics and the simple total load–sediment transport relation. The model is rudimentary in that it does not account for infiltration, sediment storage, settling lag, advection of sediment from the surf zone or bed shear stress; the importance of such effects on beach-face evolution in the swash zone has been analysed by Brocchini & Baldock (2008).

Throughout §§ 2 and 3 we develop the mathematics and numerical solution method used to model beach-face evolution over a single swash event. The absence of any

https://doi.org/10.1017/S0022112010002983 Published online by Cambridge University Press

dissipative terms is advantageous in allowing a comparison of the numerical results with the analytical solution of SM63 when the bed is rendered immobile (see Appendix C). An uncoupled analytical model based on the solution of SM63 is also detailed for comparative purposes.

In § 4 a typical 'swash event' based on initial conditions that give rise to the SM63 flow field is simulated for a mobile beach and the results are discussed in detail.

2. Mathematical model

2.1. *Governing equations*

Water motion in the swash zone is well represented by the shallow-water or long-wave model in which wavelength is considered to be much greater than water depth (Peregrine 1972). In dimensional variables the nonlinear shallow-water equations are

$$\frac{\partial \hat{h}}{\partial \hat{t}} + \hat{u}\frac{\partial \hat{h}}{\partial \hat{x}} + \hat{h}\frac{\partial \hat{u}}{\partial \hat{x}} = 0, \tag{2.1}$$

$$\frac{\partial \hat{u}}{\partial \hat{t}} + \hat{u}\frac{\partial \hat{u}}{\partial \hat{x}} + g\frac{\partial(\hat{h}+\hat{B})}{\partial \hat{x}} = 0, \tag{2.2}$$

where $\hat{h}(\hat{x},\hat{t})$ denotes the total water depth (in metres), $\hat{u}(\hat{x},\hat{t})$ denotes the depth-averaged water velocity (in metres per second), $\hat{B}(\hat{x},\hat{t})$ denotes the beach surface level (in metres) and g is the acceleration due to gravity (in metres per square seconds). Morphological evolution of the beach face is described by a sediment continuity (or Exner) equation of the form

$$\frac{\partial \hat{B}}{\partial \hat{t}} + \xi\frac{\partial \hat{q}}{\partial \hat{x}} = 0. \tag{2.3}$$

Here $\hat{q}$ is the horizontal sediment flux (in square metres per second) and $\xi = 1/(1-p)$, with p being beach porosity. To obtain closure of the governing equations (2.1)–(2.3), it is necessary to specify the sediment flux $\hat{q} = \hat{q}(\hat{u},\hat{h})$ or $\hat{q} = \hat{q}(\hat{u})$. In the present study, a simplified sediment flux is used in which $\hat{q} = \hat{q}(\hat{u})$ only, such that

$$\hat{q} = A\hat{u}^3, \tag{2.4}$$

where A is a dimensional constant (in square seconds per metre). There remains a great deal of uncertainty regarding suitable formulae for the parametrization of swash-zone sediment transport. Although a simple cubic velocity power law for $\hat{q}$ has been shown to be a good descriptor of sediment transport in the swash by certain researchers (see, e.g., Butt *et al.* 2004 and Hsu & Raubenheimer 2006), power-law-based formulae have been criticized by others (Puleo, Butt & Plant 2005). The use of such a formula is motivated here primarily by its simplicity and consequent amenability for analytical treatment. Substituting (2.4) into (2.3) and applying the chain rule gives

$$\frac{\partial \hat{B}}{\partial \hat{t}} + 3A\xi\hat{u}^2\frac{\partial \hat{u}}{\partial \hat{x}} = 0. \tag{2.5}$$

2.2. *Uncoupled and fully coupled models*

In the uncoupled approach, the hydrodynamics are divorced from the morphological evolution such that the beach face is updated (or net sediment flux calculated) only at the end of each swash event, based on net sediment flux gradient at each point.

https://doi.org/10.1017/S0022112010002983 Published online by Cambridge University Press

Therefore, the SM63 solution can be used to provide values for the hydrodynamic variables. Following PH05, (2.5) is then integrated at each point across the beach between the inundation and denudation times ($\hat{t}_i(\hat{x})$ and $\hat{t}_d(\hat{x})$, respectively). This allows us to compute the net sediment flux, $\hat{Q}(\hat{x})$, over the entire swash cycle and then update the beach profile accordingly (see § 3.1). We note that, as the bed is not updated during the swash event, for a plane sloping beach, the term $\partial\hat{B}/\partial\hat{x} =$ constant $= \tan\beta$ in (2.2).

For the fully coupled model, the shallow-water and bed-evolution equations are solved simultaneously by employing the numerical technique described in § 3.2. In this model, the evolution of the beach face has a direct and immediate impact on the hydrodynamics.

2.3. *Characteristic decomposition of the shallow-water equations*

Using standard techniques (e.g. Stoker 1957), a combination of the shallow-water equations can be found such that derivatives of the two dependent variables can be combined into derivatives in a single characteristic direction. Thus, (2.1) and (2.2) can be re-written in characteristic form as

$$\frac{\mathrm{d}(\hat{u} + 2\hat{c} + \tan\beta g\hat{t})}{\mathrm{d}\hat{t}} = \frac{\mathrm{d}R^+}{\mathrm{d}\hat{t}} = 0 \quad \text{along} \quad \frac{\mathrm{d}\hat{x}}{\mathrm{d}\hat{t}} = \hat{u} + \hat{c}, \tag{2.6}$$

and

$$\frac{\mathrm{d}(\hat{u} - 2\hat{c} + \tan\beta g\hat{t})}{\mathrm{d}\hat{t}} = \frac{\mathrm{d}R^-}{\mathrm{d}\hat{t}} = 0 \quad \text{along} \quad \frac{\mathrm{d}\hat{x}}{\mathrm{d}\hat{t}} = \hat{u} - \hat{c}, \tag{2.7}$$

where $\hat{c} = (g\hat{h})^{1/2}$. Equations (2.6) and (2.7) are the well-known characteristic equations for one-dimensional inviscid hydrodynamic flow and state that the quantities $\hat{u} \pm 2\hat{c} + \tan\beta g\hat{t}$ (the Riemann invariants) remain constant along the corresponding characteristic lines whose local gradients are given by $\mathrm{d}\hat{x}/\mathrm{d}\hat{t} = \hat{u} \pm \hat{c}$. We denote these characteristics as the $C^{\pm}$ families of characteristics.

2.4. *Characteristic decomposition of the shallow water–Exner system*

To derive a system equivalent to (2.6) and (2.7), we seek a combination of the governing equations such that derivatives of the three dependent variables can be combined to yield derivatives in a single direction (see Courant & Friedrichs 1976). The details, which are straightforward, are given in Kelly & Dodd (2009). The characteristic directions are $\mathrm{d}\hat{x}/\mathrm{d}\hat{t} = \lambda_k$, where λ_k is given by

$$\lambda_k^3 - 2\hat{u}\lambda_k^2 + [\hat{u}^2 - g(\hat{h} + 3A\xi\hat{u}^2)]\lambda_k + 3A\xi g\hat{u}^3 = 0, \tag{2.8}$$

for $k = 1, 2, 3$. The compatibility or Riemann equations along these characteristics are

$$\frac{\mathrm{d}\hat{u}}{\mathrm{d}\hat{t}} + \frac{g}{(\lambda_k - \hat{u})}\frac{\mathrm{d}\hat{h}}{\mathrm{d}\hat{t}} + \frac{g}{\lambda_k}\frac{\mathrm{d}\hat{B}}{\mathrm{d}\hat{t}} = 0. \tag{2.9}$$

For physically realistic situations, i.e. with $\hat{h} \geqslant 0$, it can be shown that the discriminant of (2.8) is less than zero (Hudson & Sweby 2003). The governing equations are therefore hyperbolic with real wave speeds (eigenvalues, λ_k). These can be found directly from (2.8) using Cardano's formula (see Abramowitz & Stegun 1965).

Letting $A \to 0$ leads to recovery of the purely hydrodynamic C^- and C^+ wave speeds, as described in § 2.3. The bed-deformation speed (λ_3), which belongs to the C_b family of characteristics, then becomes zero.

https://doi.org/10.1017/S0022112010002983 Published online by Cambridge University Press

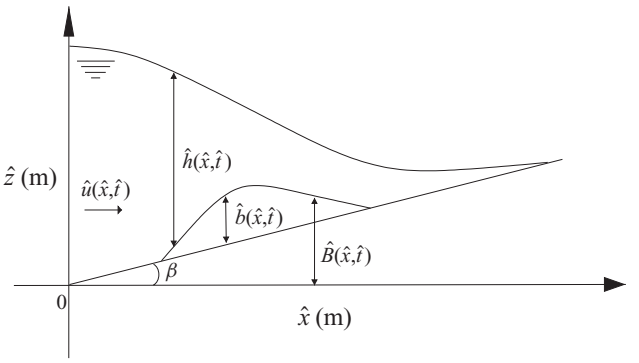


FIGURE 1. Schematic of the swash lens showing notation.

2.5. *Flow at and immediately behind the shoreline*

For the fixed-bed case, it is well known that, at the shoreline, $\hat{h} \to 0$, so that both characteristic directions $\mathrm{d}\hat{x}/\mathrm{d}\hat{t} \to \hat{u}$, such that the equation system degenerates from hyperbolic to parabolic (Hibberd & Peregrine 1979). It is also known (Peregrine & Williams 2001) that, at the tip of the swash lens, $\partial\hat{h}/\partial\hat{x} = 0$, so that the tip $\hat{x}_S$ can be described by the simple ballistic model:

$$\frac{\mathrm{d}^2\hat{x}_S}{\mathrm{d}\hat{t}^2} = -g\tan\beta. \tag{2.10}$$

The quasi-analytical solution of Kelly & Dodd (2009) for the mobile (initially) flat-bed dam-break governed by (2.1), (2.2) and (2.5) shows that $\hat{h} \to 0$ here too; they provide asymptotic forms for λ_k:

$$\lambda_3 = \hat{u}, \tag{2.11}$$

$$\lambda_1 = -\frac{(\hat{u}^2 + 12A\xi g\hat{u}^2)^{1/2} - \hat{u}}{2}, \tag{2.12}$$

and

$$\lambda_2 = \hat{u} + \frac{(\hat{u}^2 + 12A\xi g\hat{u}^2)^{1/2} - \hat{u}}{2}, \tag{2.13}$$

giving the relationship

$$\lambda_3 = \lambda_1 + \lambda_2. \tag{2.14}$$

Thus, it follows that, unlike the fixed-bed case, with $\hat{q} = A\hat{u}^3$, the fully coupled system remains hyperbolic at the shoreline. Note that the trajectory of the shoreline follows the path of a C_b characteristic. On the shoreline characteristic, (2.2) becomes

$$\frac{\mathrm{d}^2\hat{x}_S}{\mathrm{d}\hat{t}^2} = -g\left.\frac{\partial\hat{h}}{\partial\hat{x}}\right|_{\hat{x}=\hat{x}_S} - g\left.\frac{\partial\hat{b}}{\partial\hat{x}}\right|_{\hat{x}=\hat{x}_S} - g\tan\beta, \tag{2.15}$$

where $\hat{b}$ is the deviation of the bed from its initially plane slope, $\tan\beta$ (see figure 1). It can be seen that $g\partial\hat{h}/\partial\hat{x}$ and $g\partial\hat{b}/\partial\hat{x}$ provide modifications to the force at the tip, and so, in general, will alter its trajectory.

In the vicinity of the shoreline (limit $\hat{h} \to 0$), we can expand λ_3 as

$$\lambda_3 = \lambda_{(0)} + \hat{h}\lambda_{(1)} + \hat{h}^2\lambda_{(2)} + O(\hat{h}^3), \tag{2.16}$$

https://doi.org/10.1017/S0022112010002983 Published online by Cambridge University Press

where $\lambda_{(0)} = \hat{u}$. Then, collecting terms of up to second order in $\hat{h}$, we find that

$$\lambda_{(1)} = -\frac{1}{3A\xi\hat{u}}, \tag{2.17}$$

$$\lambda_{(2)} = \frac{1 + 3A\xi g}{27A^3 g\xi^3\hat{u}^3}, \tag{2.18}$$

which is valid for all the swash events, except at maximum run-up ($\hat{u}(\hat{x}_S) = 0$).

3. Solution techniques

3.1. *Uncoupled model – SM63 analytical solution*

As discussed earlier, the only known explicit exact analytical solution to the shallow-water equations (2.1) and (2.2) that has a bore as the forcing mechanism was found by SM63. The SM63 solution was derived using only seaward boundary data from the domain of dependence of the shoreline singularity, i.e. the region between the bore path and the limiting characteristic (refer to figure 1 of SM63). As such, the solution is strictly valid only in the region close to the moving shoreline, although it is a legitimate explicit solution of (2.1) and (2.2) throughout the swash zone (Peregrine & Williams 2001). The flow field in a large proportion of the interior of the swash lens is dependent on specific seaward boundary conditions. This was investigated further by Guard & Baldock (2007) (see also Baldock *et al.* 2008 and Pritchard *et al.* 2008). The SM63 solution implies that when bore-driven swash is modelled using a fixed-bed approach, then the entire motion of the swash event close to the (moving) shoreline is determined by conditions at the point of bore collapse. This is true until the formation of a singularity in the interior of the swash lens; this singularity follows a path in the physical plane known as a limit line. For the fixed-bed case, the existence of such a singularity was predicted by Shen & Meyer (1963), and it was later shown by Hibberd & Peregrine (1979) that the singularity is realized physically through the formation of a backwash bore. In particular, a single free parameter, the bore velocity at the initial shoreline position $\hat{U}_b$, is responsible for determining the maximum extent of the run-up in accordance with elementary energy (ballistics) concepts (see (2.10)). It can then be deduced that the maximum shoreline position $\hat{x}_{Smax}$ is given by

$$\hat{x}_{Smax} = \frac{\hat{U}_b^2}{2g\tan\beta}. \tag{3.1}$$

As noted by Peregrine & Williams (2001), the SM63 solution is an exact solution for the dam-break initial-value problem in which

$$\left.\begin{aligned}\hat{h}(\hat{x}, 0) &= h_0\\ \hat{u}(\hat{x}, 0) &= 0\end{aligned}\right\} \quad \text{for all} \quad \hat{x} \leqslant 0, \tag{3.2}$$

and

$$\left.\begin{aligned}\hat{h}(\hat{x}, 0) &= 0\\ \hat{u}(\hat{x}, 0) &= 0\end{aligned}\right\} \quad \text{for all} \quad \hat{x} > 0. \tag{3.3}$$

It is therefore equivalent to the Ritter (1892) dam-break solution in an accelerated reference frame (see Watson, Peregrine & Toro 1992 for details). For the dam-break problem corresponding to a bore-collapse event, the initial particle velocity (at the instant of collapse) at the leading edge is given by $2(gh_0)^{1/2}$, where h_0 is the initial

https://doi.org/10.1017/S0022112010002983 Published online by Cambridge University Press

water depth behind the dam (see, e.g., Stoker 1957). Thus,

$$\hat{x}_{Smax} = \frac{2h_0}{\tan\beta}. \tag{3.4}$$

In dimensional variables the SM63 analytical solution is

$$\hat{h}(\hat{x},\hat{t}) = \frac{(4(gh_0)^{1/2}\hat{t} - g\hat{t}^2\tan\beta - 2\hat{x})^2}{36g\hat{t}^2}, \tag{3.5}$$

and

$$\hat{u}(\hat{x},\hat{t}) = \frac{2((gh_0)^{1/2}\hat{t} - g\hat{t}^2\tan\beta + \hat{x})}{3\hat{t}}. \tag{3.6}$$

Expressions for the inundation and denudation times ($\hat{t}_i$ and $\hat{t}_d$, respectively) at a specific cross-shore location $\hat{x}$ can be obtained by setting (3.5) equal to zero and solving the resulting quadratic, yielding

$$\hat{t}_i = \frac{4(gh_0)^{1/2} - (16h_0g - 8\hat{x}g\tan\beta)^{1/2}}{2g\tan\beta}, \tag{3.7}$$

and

$$\hat{t}_d = \frac{4(gh_0)^{1/2} + (16h_0g - 8\hat{x}g\tan\beta)^{1/2}}{2g\tan\beta}. \tag{3.8}$$

The instantaneous sediment flux $\hat{q}(\hat{x},\hat{t})$ is then

$$\hat{q}(\hat{x},\hat{t}) = \frac{8A}{27}\frac{\left((gh_0)^{1/2}\hat{t} - g\hat{t}^2\tan\beta + \hat{x}\right)^3}{\hat{t}^3}, \tag{3.9}$$

and, following PH05, the net flux $\hat{Q}$ (for any $\hat{x}$) over a swash event is

$$\hat{Q}(\hat{x}) = \int_{\hat{t}_i(\hat{x})}^{\hat{t}_d(\hat{x})} \hat{q}(\hat{u})\,\mathrm{d}\hat{t} = A\int_{\hat{t}_i(\hat{x})}^{\hat{t}_d(\hat{x})} \hat{u}^3\,\mathrm{d}\hat{t}. \tag{3.10}$$

Thus, the net bed change after the event is

$$[\hat{B}]_{\hat{t}_i(\hat{x})}^{\hat{t}_d(\hat{x})} = -\xi\frac{\mathrm{d}\hat{Q}}{\mathrm{d}\hat{x}} = -\xi\left(\int_{\hat{t}_i(\hat{x})}^{\hat{t}_d(\hat{x})}\frac{\partial\hat{q}}{\partial\hat{x}}\,\mathrm{d}\hat{t} + \hat{q}(\hat{x},\hat{t}_i)\frac{\mathrm{d}\hat{t}_i(\hat{x})}{\mathrm{d}\hat{x}} - \hat{q}(\hat{x},\hat{t}_d)\frac{\mathrm{d}\hat{t}_d(\hat{x})}{\mathrm{d}\hat{x}}\right). \tag{3.11}$$

Note that

$$\hat{q}(\hat{x},\hat{t}_i)\frac{\mathrm{d}\hat{t}_i(\hat{x})}{\mathrm{d}\hat{x}} - \hat{q}(\hat{x},\hat{t}_d)\frac{\mathrm{d}\hat{t}_d(\hat{x})}{\mathrm{d}\hat{x}} = A\hat{u}^2(\hat{t}_i) - A\hat{u}^2(\hat{t}_d) = \hat{V}(\hat{t}_i) - \hat{V}(\hat{t}_d), \tag{3.12}$$

where $\hat{V}$ is a volume of sediment per unit area, so that $\hat{V}(\hat{t}_i) - \hat{V}(\hat{t}_d)$ represents the change in bed elevation for any $\hat{x}$ as the shoreline passes. For the SM63 event on a fixed bed, this term is identically zero, due to the symmetry of the tip over the uprush and backwash. For an SM63 event on a mobile bed, this will not necessarily be so, particularly because of the presence of a bed shock at the tip; the numerical solution, however, shows this term to be small compared to the main flux divergence term.

3.2. *Fully coupled model – numerical solution*

The full set of equations (2.1), (2.2) and (2.5) describing both the water and the sediment motion are solved simultaneously using a method of characteristics (MOC) based numerical scheme. This method is particularly suitable for obtaining high accuracy in problems where shocks develop, and can therefore be used to investigate

https://doi.org/10.1017/S0022112010002983 Published online by Cambridge University Press

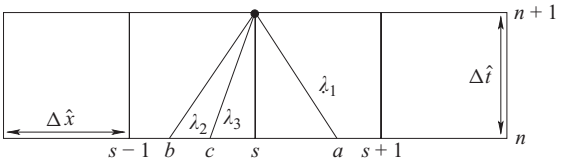


FIGURE 2. Schematic diagram showing characteristics of the computational grid.

some fundamental problems of fluid flow and geophysics with a high degree of confidence. The solution technique employed here belongs to the specified time interval (STI) class of MOC schemes first outlined for an unsteady mobile-bed flow by Wu (1973) and discussed in more detail by Lai (1986). The Riemann equations (2.9) are put into Euler difference form and integrated numerically on a regular $\hat{x} - \hat{t}$ grid with spatial increments of $\Delta\hat{x}$ and time step $\Delta\hat{t}$. Referring to figure 2 the difference equations used are

$$(\hat{u}_{s,n+1} - \hat{u}_i) + \frac{g}{(\lambda_{k,i} - \hat{u}_i)}(\hat{h}_{s,n+1} - \hat{h}_i) + \frac{g}{\lambda_{k,i}}(\hat{B}_{s,n+1} - \hat{B}_i) = 0, \tag{3.13}$$

where $i = a, b, c$ and $k = 1, 2, 3$. With the initial conditions for each time step labelled only by their spatial location ($i = a, b, c$), in the main body of the flow, the solution procedure is as follows.

(a) Assume that the slope of each of the three characteristic families at $(s, n+1)$ is equal to that at (s, n).

(b) Find the locations of a, b and c using extrapolation backwards in time.

(c) First approximations for the dependent variables ($\hat{h}$, $\hat{u}$ and $\hat{B}$) at $(s, n+1)$ are then computed using linearly interpolated values of $\hat{h}$, $\hat{u}$ and $\hat{B}$ at a, b and c in (3.13).

(d) These new values of $\hat{h}$ and $\hat{u}$ are used in the characteristic equations to recalculate the characteristic slope at $(s, n+1)$.

The above procedure is repeated until successive values of dependent variables at $(s, n+1)$ agree within a specified error limit. We note that the scheme must satisfy the Courant–Friedrichs–Lewy (CFL) stability criterion so that

$$\left|\frac{\Delta\hat{t}}{\Delta\hat{x}}\right| \leqslant \frac{1}{|\lambda_{max}|}, \tag{3.14}$$

where λ_{max} is the maximum wave speed found. If shocks are initially present in the flow, or embedded shocks develop at some later time, the scheme utilizes explicit shock fitting procedures. The shock detection and fitting procedures employed in the STI MOC scheme are outlined in Appendix B.

Handling of the upstream boundary is simplified by ensuring that the upstream domain is sufficiently long that the tail of the rarefaction fan moves unhindered until all the backwash has retreated past the initial shoreline position. Treatment of the wet–dry (shoreline) boundary is more complex and is detailed in Appendix A.

3.3. *Initial time step – Riemann wave solution*

For the initial conditions (at $\hat{t} = 0$) described by (3.2), the initial characteristic directions are ill-defined. Therefore, the MOC solution is started at an initially small time ($\hat{t}_I$). Values of the dependent variables at $\hat{t}_I$ are provided by the flat-mobile-bed Riemann wave solution of Kelly & Dodd (2009). This practice of starting at a finite time is necessary when MOC schemes are used to solve dam-break problems. On a non-erodible bed, MOC solvers are typically initialized using the Ritter solution even

https://doi.org/10.1017/S0022112010002983 Published online by Cambridge University Press

when the dam-break in question occurs on a sloping bed (see, e.g., Sakkas & Strelkoff 1973).

The validity of using initial values derived for the flow over a horizontal bed for sloping-bed problems does not appear to have been discussed previously, and is investigated here by letting $\hat{B}(\hat{x},\hat{t}) = \hat{x}\tan\beta + \hat{b}(\hat{x},\hat{t})$ and by introducing the following scaling:

$$x^* = \left(t_I g^{1/2} h_0^{1/2}\right)^{-1} \hat{x}, \tag{3.15}$$

$$t^* = t_I^{-1}\hat{t}, \tag{3.16}$$

$$h^* = h_0^{-1}\hat{h}, \tag{3.17}$$

$$u^* = g^{-1/2} h_0^{-1/2}\hat{u}, \tag{3.18}$$

$$b^* = (\xi A g h_0)^{-1}\hat{b}, \tag{3.19}$$

where asterisks denote scaled non-dimensional variables. Substituting these new scaled variables into the governing equations (2.1), (2.2) and (2.5) gives

$$\frac{\partial h^*}{\partial t^*} + u^*\frac{\partial h^*}{\partial x^*} + h^*\frac{\partial u^*}{\partial x^*} = 0, \tag{3.20}$$

$$\frac{g^{1/2}h_0^{1/2}}{t_I}\left\{\frac{\partial u^*}{\partial t^*} + u^*\frac{\partial u^*}{\partial x^*} + \frac{\partial(h^* + A\xi g b^*)}{\partial x^*}\right\} + g\tan\beta = 0, \tag{3.21}$$

and

$$\frac{\xi A g h_0}{t_I}\left\{\frac{\partial b^*}{\partial t^*} + \frac{\partial(u^{*3})}{\partial x^*}\right\} = 0. \tag{3.22}$$

Therefore, it follows that in the limit $t_I \to 0$, i.e. immediately after the bore collapse, the term $g\tan\beta$ in (3.21) becomes negligible and the equation system approaches that of a flat bed. This approach requires that $\hat{u}$ be characterized by a finite velocity and $\hat{b}$ by a finite perturbation, with both related to the initial depth of water behind the dam; for the governing equations used here, both of these requirements are satisfied (Kelly & Dodd 2009). The same argument can also be put forward for the fixed-bed case.

4. SM63-type swash events

4.1. *Non-dimensionalization*

Here we present results in dimensionless variables that are more appropriate for the sloping beach on which the collapse initially takes place. We use the transformations

$$x = \frac{\hat{x}}{h_0\tan\beta}, \tag{4.1}$$

$$t = \hat{t}\sqrt{\frac{g}{h_0}}, \tag{4.2}$$

$$h = \frac{\hat{h}}{h_0\tan^2\beta}, \tag{4.3}$$

$$u = \frac{\hat{u}}{\sqrt{g h_0}\tan\beta}, \tag{4.4}$$

$$b = \frac{\hat{B}}{h_0\tan^2\beta} - x, \tag{4.5}$$

https://doi.org/10.1017/S0022112010002983 Published online by Cambridge University Press

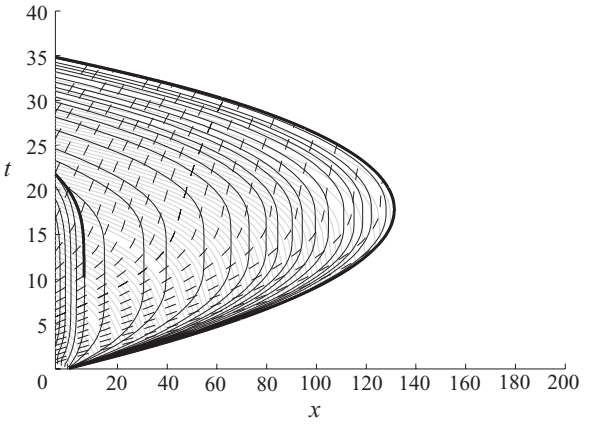


FIGURE 3. Space–time plot of selected characteristics from the three families, C^+ (black dashed), C^- (grey solid) and C_b (black solid), for an SM63-type swash event with $\sigma = 0.0654$. The shoreline and path of the sediment bore are illustrated by bold lines.

which yield the system

$$\frac{\partial h}{\partial t} + u\frac{\partial h}{\partial x} + h\frac{\partial u}{\partial x} = 0, \tag{4.6}$$

$$\frac{\partial u}{\partial t} + u\frac{\partial u}{\partial x} + \frac{\partial (h+b)}{\partial x} + 1 = 0, \tag{4.7}$$

$$\frac{\partial b}{\partial t} + 3\sigma u^2\frac{\partial u}{\partial x} = 0. \tag{4.8}$$

Here h_0 is the initial depth of water at bore collapse and

$$\sigma = A\xi g \tag{4.9}$$

is a dimensionless bed-evolution parameter. Analysis of swash-zone data (Kelly 2009) indicates that, for sand beaches, values of σ are likely to lie in the range

$$0.01 \leqslant \sigma \leqslant 0.2. \tag{4.10}$$

All calculations are run until the water has retreated back past the initial shoreline position. Determining a suitable value for A is difficult; here we utilize the field data of Masselink *et al.* (2005), collected in the swash zone of a medium sand ($D_{50} = 0.27$–0.29 mm) dissipative beach, to compute an order of magnitude estimate. Using measured values of $\hat{q}$ and $\hat{u}$ in the middle of the run-up and again in the middle of the backwash for a fixed cross-shore location, an average value of $A = 0.004\ \mathrm{s^2\,m^{-1}}$ was computed. Further, assuming $p = 0.4$ for beach porosity, a value of $\sigma = 0.0654$ is obtained from (4.9). Swash events are modelled for $\sigma = 0.0654$, and the extrema $\sigma = 0.01$ and $\sigma = 0.2$. It should be noted that the results of numerical experiments show that when the hydro- and morphodynamics are fully coupled, swash events with differing values of beach porosity and/or sediment mobility (i.e. σ) are no longer hydrodynamically identical, as they are for the uncoupled model.

4.2. *Flow structure*

Figures 3 and 4 show the characteristic grid and contours of h, u and b for $\sigma = 0.0654$. Figure 5 provides dimensional snapshots of the same swash event in order to better illustrate the salient flow features. At the moment of dam/bore collapse, there is

https://doi.org/10.1017/S0022112010002983 Published online by Cambridge University Press

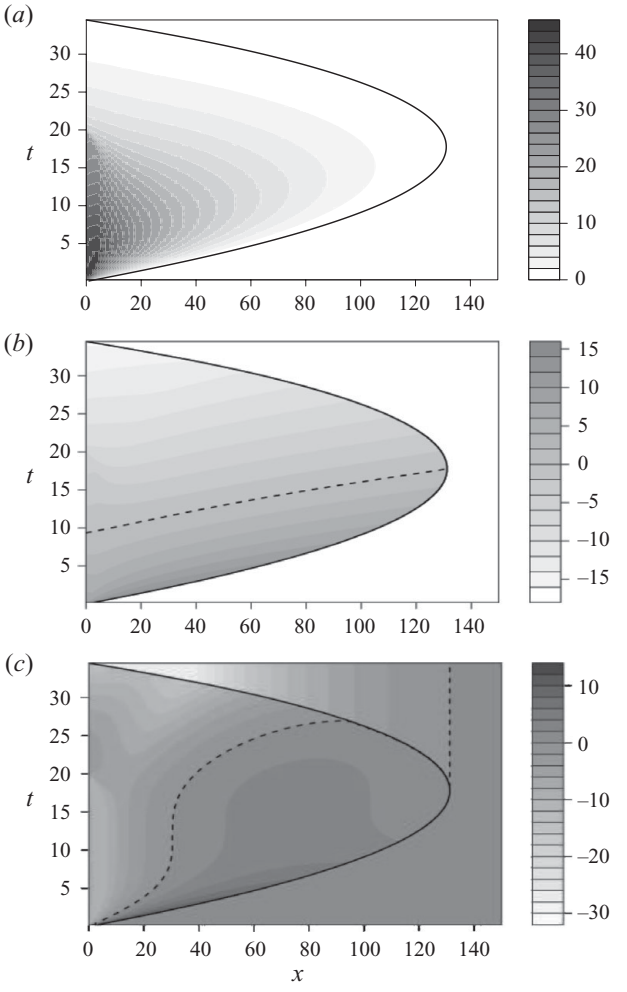


FIGURE 4. Space–time plot showing dimensionless contours of (*a*) dimensionless water depth (h), (*b*) dimensionless water velocity (u) and (*c*) change in beach profile (b) for SM63-type swash with $\sigma = 0.0654$. Dashed lines in (*b*) and (*c*) show the zero contour.

an instantaneous acceleration of water and a sediment bore forms at the shoreline. The flow is subsequently dominated by gravity and the consequent decrease in water velocity over time causes the sediment bore to progressively reduce in height as the swash climbs the beach; note that the sediment bore height is determined directly from the shock relation associated with the Exner equation in which $b \propto u$ (refer to Appendix B for details).

At flow reversal, the height of the sediment bore is momentarily zero (see figure 5*c*, *d*). The sediment bore then again begins to grow in strength as the flow at the shoreline accelerates seawards. Further back within the main body of the flow, two gradient discontinuities form in all dependent variables at the instant of dam/bore collapse; these correspond to those marking the beginning and the end of the constant-state region for the mobile-bed dam-break over an initially flat bed (see Kelly & Dodd 2009). The first of these gradient discontinuities forms, and continues to move, seawards of the initial shoreline location and is therefore outside our

https://doi.org/10.1017/S0022112010002983 Published online by Cambridge University Press

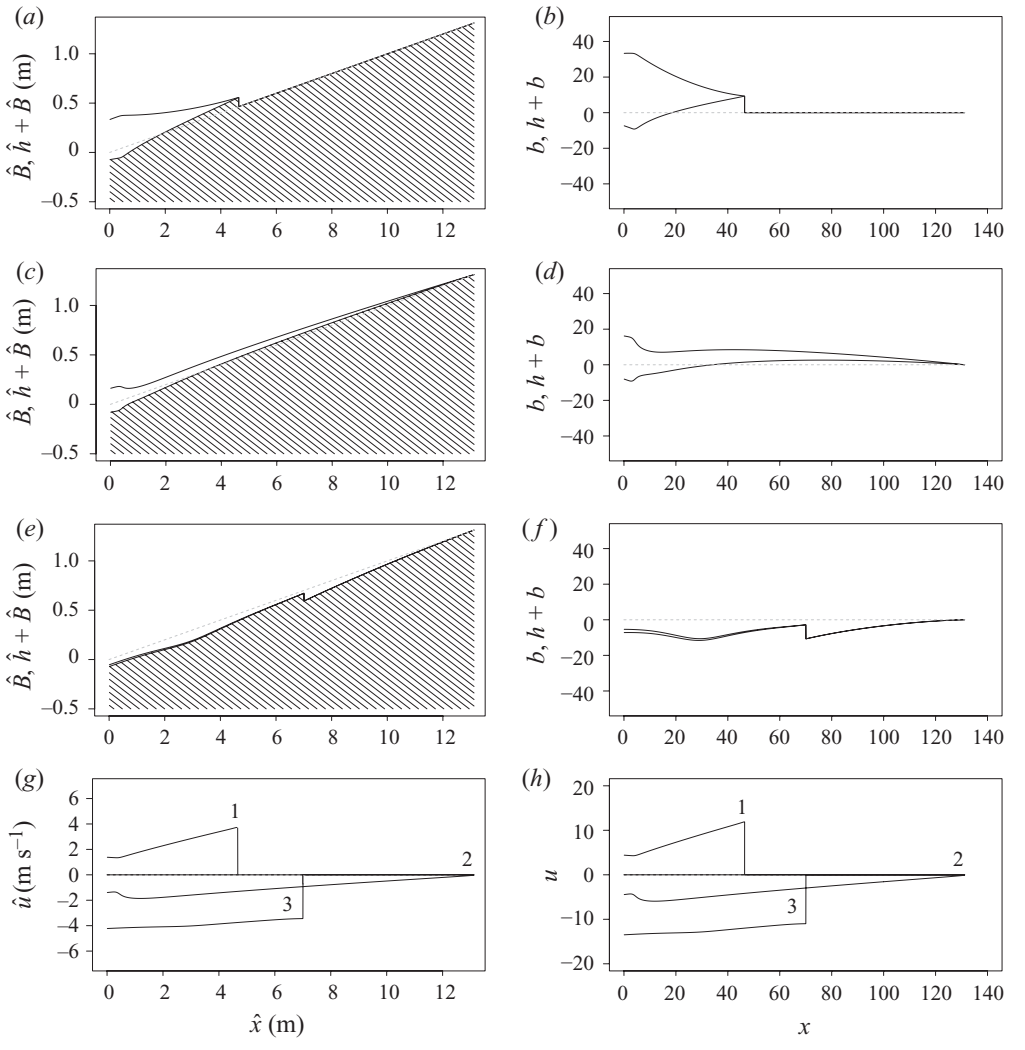


FIGURE 5. Snapshots showing (from top to bottom) salient features of the (1) run-up ($\hat{t} = 1.12$ s); (2) flow reversal ($\hat{t} = 5.72$ s); and (3) backwash ($\hat{t} = 9.42$ s) for SM63-type swash with $\sigma = 0.0654$. (*g*, *h*) The associated velocity profiles. (*a*), (*c*), (*e*) and (*g*) are dimensional, illustrating the physical situation; (*b*), (*d*), (*f*) and (*h*) are non-dimensional.

domain of interest. The second gradient discontinuity forms landwards of the initial shoreline position and climbs the beach, propagating along a characteristic until the discontinuity and the flow local to it reverse. Once the flow has reversed a compression, wave begins to build up on the downstream side of the gradient discontinuity and, as also occurs in analogous gas dynamical problems (Moretti & DiPiano 1983), this very soon develops into a shock wave. These flow features are clearly evident in the snapshots of figure 5; the characteristic grid shown in figure 3 provides further insight into the flow structure. It can be seen in figure 3 that the gradient discontinuity initially moves as a characteristic (the limit of a weak shock) and later grows into a fully developed shock. Here, the shock takes the form of a relatively slow-moving seaward-facing bed step (i.e. it forms due to the coalescence of C_b characteristics; see

https://doi.org/10.1017/S0022112010002983 Published online by Cambridge University Press

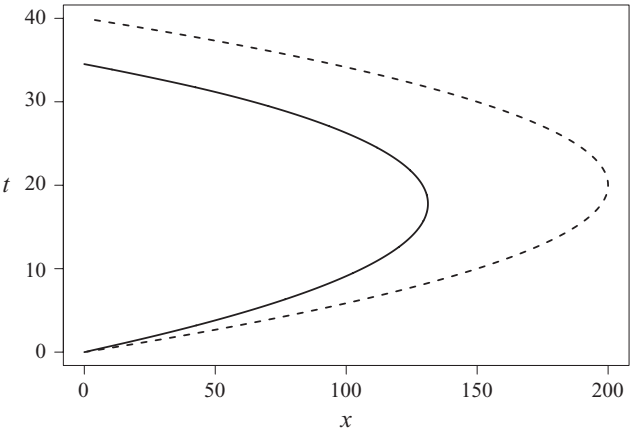


FIGURE 6. Dimensionless shoreline position in the physical plane for an SM63 swash event on a mobile beach with $\sigma = 0.0654$ (solid line). For comparison the SM63 (fixed beach) analytical shoreline motion is also shown for the same initial conditions (dashed line).

figure 5*c*, *d* for a profile view of this bed-step formation). Unlike the sediment bore at the wave tip, this moving bed step appears to be akin to the sediment bores found in steady alluvial flows (Needham & Hey 1991). The water arriving from the landward side of the slowly retreating bed step meets it almost as though it were unmoving and, similar to the flow over a fixed bed step, forms a hydraulic jump over it. With subscripts H and L denoting the high and low side of the bed shock, respectively, the strength of the shock, defined as $(B_H - B_L)/h_{min}$, where h_{min} is the minimum water depth at the shock, is relatively weak ($(B_H - B_L)/h_{min} < 1.8$ for $\sigma = 0.0654$); the change in slope of the two hydrodynamic characteristics as they cross the shock path is barely noticeable in figure 3.

Also note that if the wave structure is examined further using figure 3, it can be seen that the wave speed of the incoming (outgoing) characteristics, λ_1 (λ_2), remains positive (negative). Further, the incoming characteristics terminate at the shoreline. In fact, only the C_b characteristic (λ_3) changes sign. This characteristic represents the deformation of the bed, and, looking closely at figure 3, it can be seen that the bed is highly mobile over the leading edge of the uprush, and for a significant proportion (in fact, the majority) of the backwash (see figure 4).

4.3. *Maximum run-up and beach-face evolution*

Figure 6 shows the position of the shoreline in the physical plane for the swash event of figure 4, and also shows the equivalent shoreline for the same bore collapse on a fixed beach. The limiting effect of bed mobility on run-up is fairly severe with the maximum run-up of the coupled model only around 70 % of the uncoupled solution. A lower tip velocity at the point of bore collapse (compared to that obtained from the fixed-bed problem) is partly responsible for this decrease in maximum run-up; however, the flow dynamics are also more complex than in the fixed-bed case. Interestingly, over a mobile bed, maximum run-up is greater than that expected from the ballistics theory prediction based on the morphodynamic initial tip velocity. Other physical variables at the tip are shown in figure 7.

It can be seen that the bore height decays rapidly as the sediment bore proceeds up the beach. Of particular interest is the tip velocity ($u(x_S)$), which is approximately a straight line, indicating that the shoreline motion is still (to leading order) parabolic,

https://doi.org/10.1017/S0022112010002983 Published online by Cambridge University Press

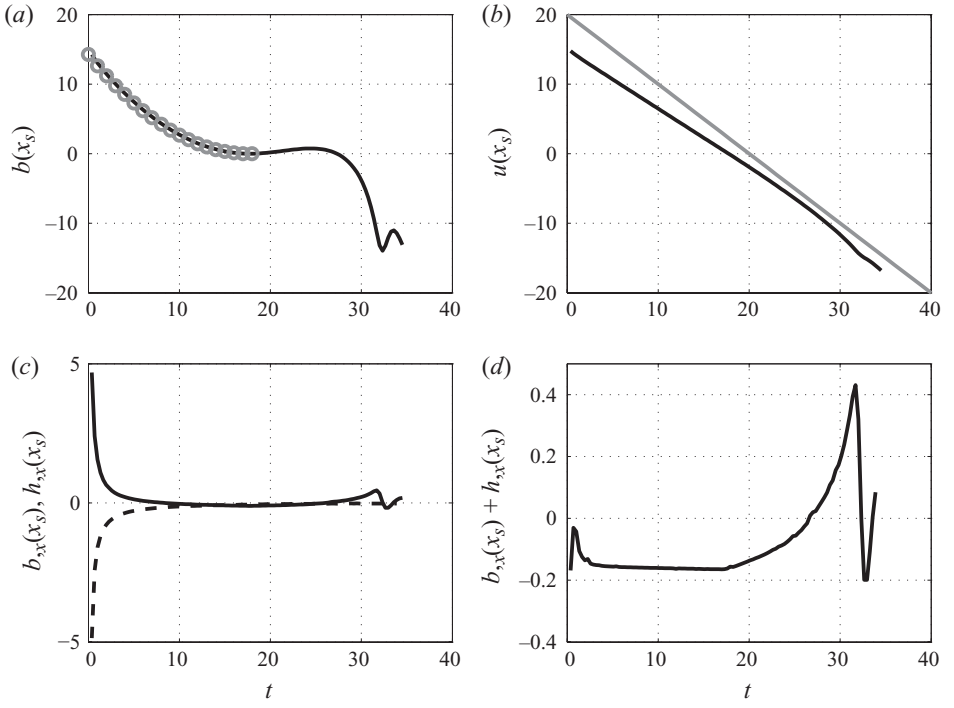


FIGURE 7. Shoreline variables during the swash event. (*a*) Sediment bore height calculated from the numerical model (solid black line) and from (4.11) (grey circles), with b_i given by the sediment bore height calculated from the Riemann solution of Kelly & Dodd (2009) at initial time, and $\partial b/\partial x|_{x=x_S} + \partial h/\partial x|_{x=x_S} = -0.162$. (*b*) Fluid and shoreline velocities; the grey line indicates $u(x_S)$ for the equivalent fixed-bed bore collapse. (*c*) $\partial b/\partial x$ and $\partial h/\partial x$ (dashed line). (*d*) $(\partial h/\partial x) + (\partial b/\partial x)$.

despite the fact that $\partial h/\partial x|_{x=x_S}$ and $\partial b/\partial x|_{x=x_S}$ are non-zero. The reason for this can be seen in figure 7(*d*), in which the effects of bed and water slope produce a quasi-constant modification to gravity for the uprush (see (2.15)), so that the effect is to produce an additional onshore force (hence the slightly smaller slope for the $u(x_S)$ line than that for the fixed-bed case; see figure 7*b*). This is also the reason why the fixed-bed event for the same initial velocity produces a smaller run-up. The conclusion is that it is at the first instant of bore collapse from the initial conditions (3.2) and (3.3) to the Riemann solution of Kelly & Dodd (2009) that the initial tip velocity and therefore the maximum run-up is determined, as for the solution of SM63 and Peregrine & Williams (2001). Further note that $\partial b/\partial x|_{x=x_S} < 0$ for $t > 8.4$, indicating that a mound of sediment accumulates behind the diminishing sediment bore, which ultimately results in deposition at the head of the beach at maximum run-up; see figure 5(*c*, *d*). Note the bed elevation at the tip in the backwash (figure 7*a*), where the water initially retreats back over the berm that was deposited during the uprush, thus stripping sediment as the bore now retreats offshore. The final 'kink' in the profile originates from the shoreward bed gradient discontinuity. The deviation from a purely parabolic profile is clear in the backwash, as seen in figure 7(*b*). Figure 7(*d*) also shows the time evolution of $\partial h/\partial x|_{x=x_S} + \partial b/\partial x|_{x=x_S}$ for the whole swash event. For small t ($t < 1$), it is possible that there is some numerical inaccuracy as $\partial h/\partial x|_{x=x_S} + \partial b/\partial x|_{x=x_S}$ initially increases sharply, because as $t_I \to 0$, the

https://doi.org/10.1017/S0022112010002983 Published online by Cambridge University Press

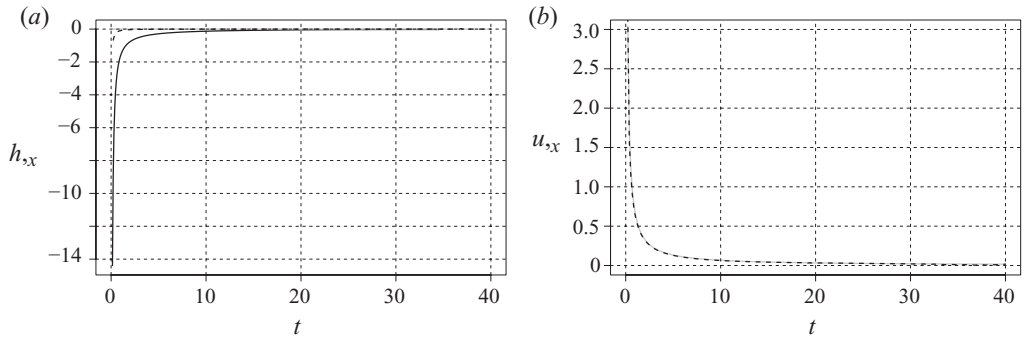


FIGURE 8. Variation of $\partial h/\partial x|_{x=x_S}$ (*a*) and $\partial u/\partial x|_{x=x_S}$ (*b*) during the run-up from the numerical MOC solution over the full swash event when $\sigma = 0.0654$ (solid line). For comparison the numerical (dashed line) and the SM63 analytical (grey line) values are also shown for the fixed-bed case ($\sigma = 1 \times 10^{-10}$).

flat-bed solution is recovered (see (3.15)–(3.19)), wherein $\partial h/\partial x|_{x=x_S} + \partial b/\partial x|_{x=x_S} = 0$ (because otherwise the shock tip would accelerate without bound; this also follows from the theory of generalized simple waves, according to Jeffrey 1976); see also Kelly & Dodd (2009).

Note that this is apparent here because to a leading order in the early run-up, $\partial h/\partial x|_{x=x_S}$ and $\partial b/\partial x|_{x=x_S}$ cancel each other out. In the backwash, the origin of the non-parabolic tip behaviour(see figure 7*b*) becomes clear.

In figure 8 we show $\partial h/\partial x$ and $\partial u/\partial x$ at the tip computed from the numerical MOC values. This figure also shows the values for the SM63 analytical solution and their numerical equivalents using the present numerical approach. It can be seen that the numerical values are very close to those obtained from the analytical solution (3.5) and (3.6); further, $\partial h/\partial x|_{x=x_S} < 0$ for the whole swash event.

Finally, (2.15) can be rewritten using the shock relation (B 3) (or from the Riemann equation (2.9), and (2.16)–(2.18)) as

$$\frac{1}{b_S^{1/2}}\frac{\mathrm{d}b_S}{\mathrm{d}t} = -2\sigma^{1/2}\left(\tan\beta + \left.\frac{\partial h}{\partial x}\right|_{x=x_S} + \left.\frac{\partial b}{\partial x}\right|_{x=x_S}\right), \tag{4.11}$$

where $b_S = b\ (x = x_S)$. It can be seen that the bed-shock-height decay can therefore be a result of a constant force at the tip, depending on the rate of decay. Assuming that $\partial h/\partial x|_{x=x_S} + \partial b/\partial x|_{x=x_S}$ is indeed constant allows integration of (4.11) such that

$$b_S = b_I - 2\sigma^{1/2} b_I^{1/2}\tan\beta' t + \sigma\tan^2\beta' t^2, \tag{4.12}$$

where b_I is the initial bore height and $\tan\beta' = \tan\beta + (\partial h/\partial x|_{x=x_S}) + \partial b/\partial x|_{x=x_S}$. If we take b_I from the Riemann solution of Kelly & Dodd (2009) at the initial time, and $\partial h/\partial x|_{x=x_S} + \partial b/\partial x|_{x=x_S} = -0.162$, this being the limiting value in figure 7(*d*), we can see that the resulting decay in bore height is essentially identical to that from the numerical solution (figure 7*a*).

The sediment bore at the tip is an extremely effective transporter of sediment. When flow reverses at the tip, initially it does not accelerate as quickly as it would on a fixed beach, as the stoss side of the berm reduces the local beach gradient; we note that it does not reverse the overall local gradient – a condition that would lead to a pool of water being left at the upper limit of the swash zone – only the local $\partial b/\partial x|_{x=x_S}$ reverses sign (see figure 7*c*). Water in the backwash strips sediment

https://doi.org/10.1017/S0022112010002983 Published online by Cambridge University Press

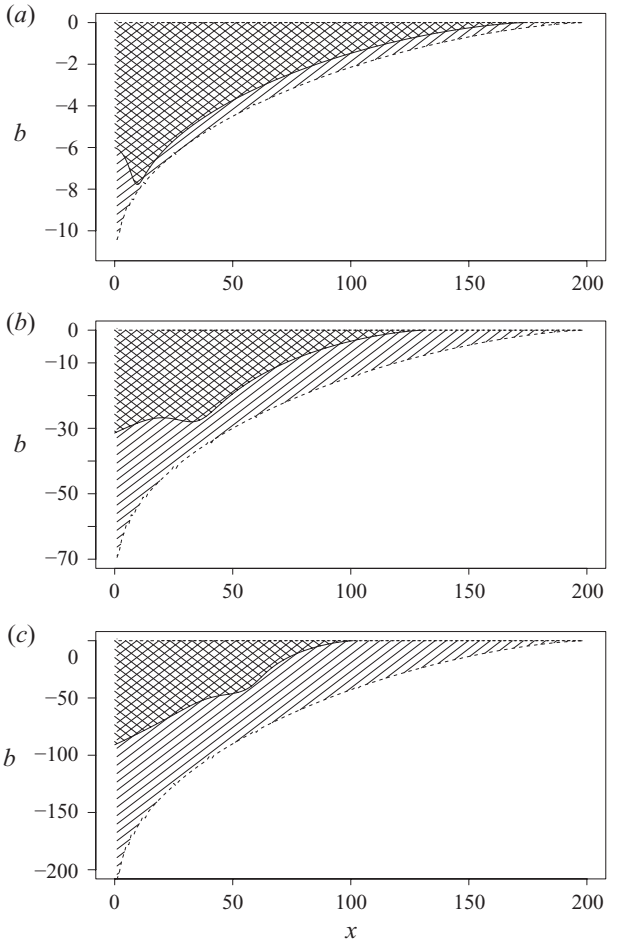


FIGURE 9. Dimensionless change in bed level relative to the initially plane beach (denoted by b) for uncoupled (dashed and shaded) and fully coupled (solid and hashed) transport models after one swash cycle for $\sigma = 0.01$ (a), $\sigma = 0.0654$ (b) and $\sigma = 0.2$ (c).

from the beach as it retreats over the berm and, as the sediment bore at the tip gets progressively stronger with increasing offshore velocity at the tip, the amount of sediment stripped off the beach in the backwash increases as the original shoreline position is approached.

4.4. *Relationship between final beach profile and bed-evolution parameter (σ)*

Figure 9 illustrates the bed change for both coupled and uncoupled beach evolution for $\sigma = 0.01, 0.0654$ and 0.2. It is immediately obvious, within the range of σ values being considered, that coupling leads to a significant reduction in the amount of sediment stripped from the beach. Moreover, as σ increases, there is a growing disparity between the coupled and uncoupled predictions of beach-face change and maximum run-up; this finding emphasizes the importance of coupling when modelling flow over beaches that exhibit a high degree of sediment mobility. It is worth pointing out that the use of a lower value of A, and thus σ, in the backwash in the coupled model, as suggested by a number of researchers (see, for example, Masselink & Li 2001

https://doi.org/10.1017/S0022112010002983 Published online by Cambridge University Press

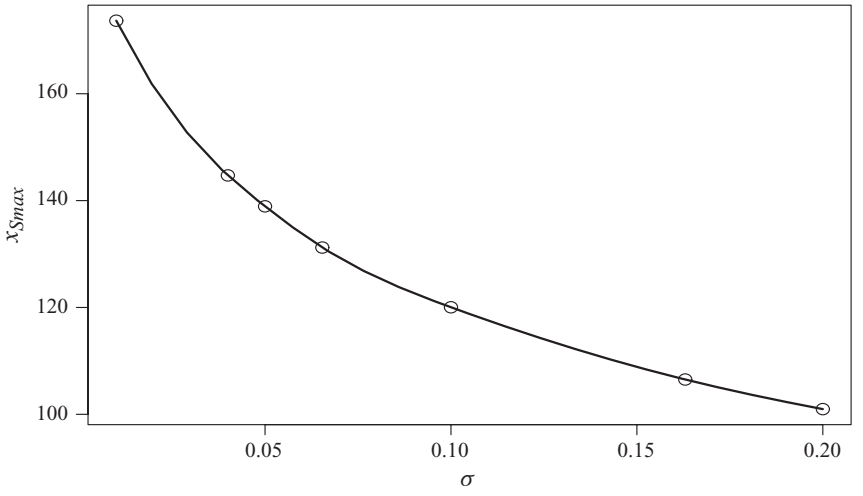


FIGURE 10. The effect of varying the bed-evolution parameter (σ) on maximum run-up (x_{Smax}).

and Masselink *et al.* 2005), would further decrease the net offshore transport. The limiting effect of bed evolution on run-up is shown in figure 10; the figure clearly demonstrates that coupling significantly reduces the predicted run-up for the range of σ values likely to be found on a sand beach (see § 4.1). For the maximum value of σ the maximum run-up is approximately half of what it would be on a fixed beach. (From (3.4) and (4.1), the non-dimensional value of x_{Smax} is 200 for the fixed-beach case.)

5. Concluding remarks

These new numerical MOC solutions of a fully coupled shallow water–Exner system, based on hydrodynamical initial conditions that give rise to the SM63 flow field, reveal that full coupling between flow and bed dramatically alters the pattern of beach-face evolution over a single swash event compared with predictions based on purely hydrodynamical equations employing the same sediment transport equation: $\hat{q} = A\hat{u}^3$ (see Pritchard & Hogg 2005).

Our findings support those of Dodd *et al.* (2008) in that the high-Froude-number flows of the swash mean that divorcing the hydro- and morphodynamics when modelling this region of the nearshore is inappropriate. The implications of this for the understanding and modelling of swash overtopping, run-up and breaching are profound.

Nonetheless, the details of this modelling should be viewed with some scepticism from the point of view of predictions of real beach change. This is in part because much of the onshore transport results from the initial bed shock or sediment wedge, and this is determined at the point of bore collapse (Kelly & Dodd 2009) and is discontinuous with regard to the initial conditions, in the same way as is the Ritter solution (Ritter 1892) and that examined by Pritchard & Hogg (2005). This is a consequence of the inadequacy of the shallow-water equations in describing the early stages of a dam-break/bore collapse, and is well known (see, e.g., Peregrine & Williams 2001). Furthermore, on beaches with large grain size, infiltration is known to be very important, and, in the upper swash, will contribute to accretion. Other effects (settling

https://doi.org/10.1017/S0022112010002983 Published online by Cambridge University Press

lag, injection of sediment from the surf zone, turbulence at bore collapse and bed shear stress) are also ignored here. Finally, note that the use of (2.4) is fundamental to the structure of the subsequent swash event. This formula, as has been noted previously, implies that an infinitesimally thin film of water (i.e. the tip) can transport a finite quantity of sediment (in particular, creating the sediment bore at the tip). Other such formulae that factor in the water depth will yield very different behaviour at the tip, although the structure elsewhere will be less affected.

The authors acknowledge with thanks the financial support of the Engineering and Physical Sciences Research Council. The authors wish to express their thanks to Dr S. Hibberd (Division of Applied Mathematics, University of Nottingham) for the many useful discussions concerning this work, particularly during its early stages. The help of Dr R. Briganti (Environmental Fluid Mechanics Research Centre, University of Nottingham) is also acknowledged. Finally, the constructive criticism of the original draft offered by the anonymous reviewers was appreciated by both authors.

Appendix A. Shoreline boundary conditions

Following Titov & Synolakis (1995), our treatment of the shoreline boundary uses a time-dependent space step $\Delta\hat{x}(\hat{t})$ for the last mesh point (shoreline position). However, the algorithm developed in Titov & Synolakis (1995) requires that the beach slope is known *a priori*; this criterion is not met for the mobile-bed problem when the sediment-transport formula is $\hat{q} = \hat{q}(\hat{u})$ only. Therefore, we present the following algorithm for the shoreline boundary.

A.1. *Run-up*

Assuming that at time $\hat{t}$ the location of the shoreline boundary $\hat{x} = \hat{x}_S(\hat{t}) = \hat{x}_S^{\hat{t}}$ is known, with the subscript S representing the last fixed nodal point on a beach whose slope ($\tan\beta$) is initially constant, the algorithm is summarized as follows:

(*a*) At time $\hat{t}$ the velocity at the shoreline boundary $\mathrm{d}\hat{x}_S/\mathrm{d}\hat{t} = \hat{u}_S$ is obtained by a (linear) extrapolation from the previous two (s and $s-1$) fixed nodes.

(*b*) An initial guess for $\hat{x}_S^{\hat{t}+\Delta\hat{t}}$ is made using the formula $\hat{x}_S^{\hat{t}+\Delta\hat{t}} = \hat{x}_S^{\hat{t}} + \hat{u}_S^{\hat{t}}\Delta\hat{t}$.

(*c*) $\hat{u}_S^{\hat{t}+\Delta\hat{t}}$ is computed using linear extrapolation.

(*d*) $\hat{x}_S^{\hat{t}+\Delta\hat{t}}$ is re-computed using the formula $\hat{x}_S^{\hat{t}+\Delta\hat{t}} = \hat{x}_S^{\hat{t}} + \{((\hat{u}_S^{\hat{t}+\Delta\hat{t}} + \hat{u}_S^{\hat{t}})/2)\Delta\hat{t}\}$.

(*e*) Steps (*c*) and (*d*) are repeated until values of $\hat{x}_S^{\hat{t}+\Delta\hat{t}}$ agree to within a specified error limit.

(*f*) The water depth at the shoreline boundary $\hat{h}_S$ is set equal to zero.

(*g*) The value of the bed height is set using the beach slope ($\tan\beta$) and the shock relation at the shoreline boundary, i.e.

$$\hat{B}_S = A\xi\hat{u}_S^2 + \hat{x}_S^{\hat{t}+\Delta\hat{t}}\tan\beta. \tag{A 1}$$

(*h*) If, at time $\hat{t} + \Delta\hat{t}$, the shoreline boundary position $\hat{x}_S$ exceeds the next fixed mesh point ($s+1$), the value of s is incremented by 1 and this fixed mesh point is introduced. The dependent variables are determined here by an interpolation from the values at the previous fixed mesh point ($\hat{x}_{S-1}$) and those at $\hat{x}_S$.

A.2. *Backwash*

Treatment of the backwash is almost the same as the run-up, the differences being that in step (*g*) the bed level at the tip is computed using the combination of an extrapolation procedure employing data from the previous two mesh points and the

https://doi.org/10.1017/S0022112010002983 Published online by Cambridge University Press

shock relation. In step (h) if the shoreline has receded beyond a fixed mesh point, then that mesh point is no longer used in the computational procedure.

This approach differs significantly from that of Titov & Synolakis (1995) as we track shoreline position explicitly through time using an extrapolative procedure. Titov & Synolakis use a horizontal projection of the free surface and specify the shoreline position as being where this line intercepts the beach (cf. figure 2 of their paper). Our algorithm has proven to be extremely robust when used with both the STI MOC scheme presented here and more conventional finite-difference schemes.

Appendix B. Shock fitting

When a shock is present in an otherwise continuous flow, the only mathematically sound solution of the inviscid shallow water and shallow water–Exner equations requires a perfect discontinuity. Inevitably, in shock capturing schemes, the width of a shock is grid-dependent and scaled according to the mesh spacing and the shock is therefore smeared over at least two mesh points. In this study, all shocks within the flow are dealt with explicitly and are thus resolved at a single point using a 'floating shock fitting' procedure in which the shock is allowed to wander freely between mesh points on the computational grid (see, e.g., Moretti 1973). Shock fitting requires the explicit formulation of the Rankine–Hugoniot (jump) equations, following Needham & Hey (1991). The Rankine–Hugoniot conditions for the system comprising (2.1), (2.2) and (2.5) are found from the integral form of these equations as

$$[\hat{h}(\hat{u}-\hat{w})]_L^H = 0, \tag{B 1}$$

$$\left[-\hat{w}\hat{u}\hat{h}+\hat{h}\hat{u}^2+\frac{g\hat{h}^2}{2}\right]_L^H+\frac{g}{2}(\hat{B}_H-\hat{B}_L)(\hat{h}_L+\hat{h}_H)=0, \tag{B 2}$$

$$[\hat{B}\hat{w}-A\xi\hat{u}^3]_L^H = 0, \tag{B 3}$$

where the subscripts H and L represent values at the high and low sides of a shock, respectively, and $\hat{w}$ is the (dimensional) shock velocity. As the tip follows the trajectory of a C_b characteristic, whose celerity is given by $\lambda_3=\hat{u}$ (see § 2.5), the sediment bore moves at the same velocity as the water at the tip, i.e. $\hat{w}=\hat{u}$. From (B 3), it therefore follows that $\hat{B}_H=A\xi(\hat{u}_H)^2$, that is, the height of the sediment bore at the tip is proportional to the square of the water velocity there.

B.1. *Shock detection*

In order to detect embedded shocks, we use a technique developed by Moretti (1971) for gas dynamical problems. This consists of, at the end of each time step, identifying the mesh interval $(s,\ s+1)$ where the water-depth gradient (or alternatively the bed-level gradient) is greatest. If this maximum gradient then increases in time for a prescribed number of consecutive steps (here we use five consecutive steps; however, the shock is detected only marginally later if more steps are used), a shock is placed at the mid-point of the mesh interval $(s+(1/2))$. The initial shock speed is defined as the average of the corresponding wave speeds at s and $s+1$ (i.e. $\hat{w}=0.5(\lambda_i|_s+\lambda_i|_{s+1})$). Following Moretti (1971), we note that the early detection of shocks, in which the shock initially moves as a characteristic (the limit of a weak shock), is preferable to late detection where the shock has already built up some strength.

https://doi.org/10.1017/S0022112010002983 Published online by Cambridge University Press

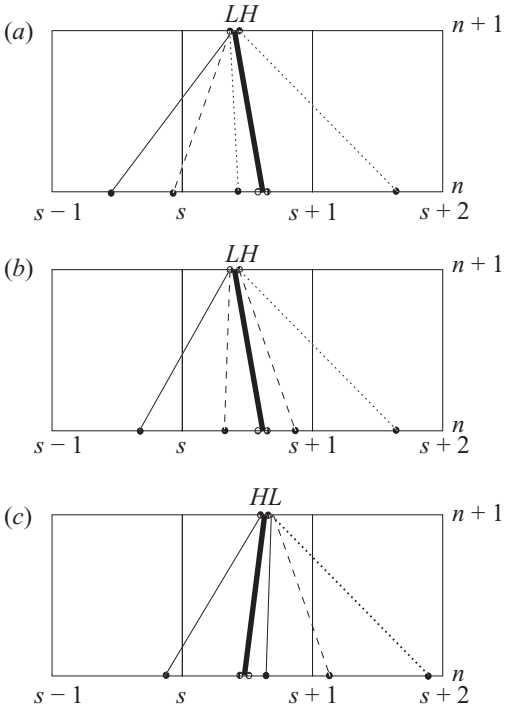


FIGURE 11. Configuration of characteristics in the $\hat{x}$–$\hat{t}$ plane corresponding to (*a*) type 1, (*b*) type 2 and (*c*) type 3 shocks. The shock path is shown by the thick line whereas C^+, C^- and C_b characteristics are represented by thin solid, dotted and dashed lines, respectively.

B.2. *Shock evolution*

In shock fitting schemes, the position of the shock must be tracked through time. Additionally, for an unsteady flow, values of all dependent variables on the high side of the shock, as well as the shock velocity, must be computed at each time step. A morphodynamic shocked flow is more complex than a pure hydrodynamic shocked flow as three distinct shock types can exist. Sieben (1997, 1999) has classified the three shock types for the shallow water–Exner system. Each shock type corresponds to a different characteristic configuration at the shock (see figure 11). The method used to fit shocks necessarily varies according to the type of shock under consideration. The following text, used in conjunction with figure 11, outlines the fitting procedures developed for use with the MOC STI scheme presented in this paper.

B.3. *Type* 1 *or type* 3 *(hydrodynamic) shock*

(*a*) An initial estimate for the new shock location $\hat{x}_w$ at $n+1$ is made using the value of the shock speed at s. This is assumed to be known in the case of a pre-existing shock or is computed by the method given above for embedded shocks.

(*b*) Values of all dependent variables ($\hat{h}$, $\hat{u}$ and $\hat{B}$) more than one mesh point away on the low and high sides of the shock are computed using the STI MOC technique.

(*c*) Values of all dependent variables ($\hat{h}$, $\hat{u}$ and $\hat{B}$) at point L on the low side of the shock are computed by the STI MOC technique.

(*d*) Using high-side values from the previous time step, an estimate of the C^- characteristic wave speed (λ_1) is arrived at at point H. Using this approximation, a

https://doi.org/10.1017/S0022112010002983 Published online by Cambridge University Press

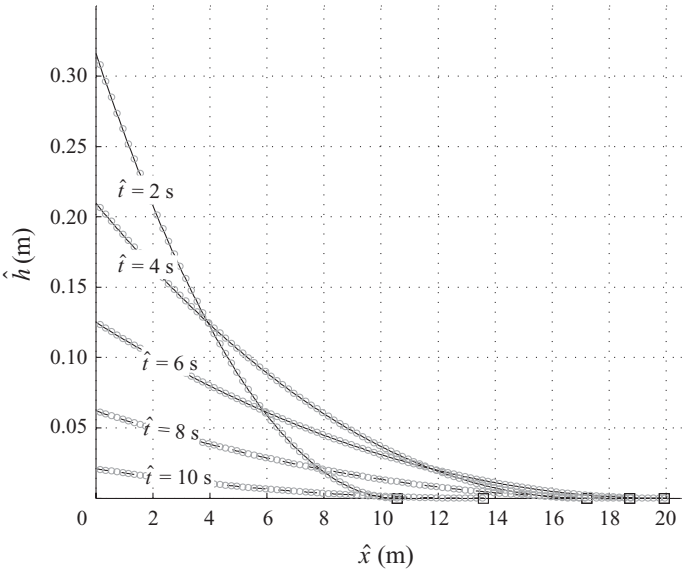


FIGURE 12. Comparison of analytical (lines) and STI MOC numerical (circles) predictions of the water depth h at dimensional times shown for the SM63 swash with $A = 1 \times 10^{-10}$ s^2 m^{-1}. Dashed lines indicate backwash and squares show the analytical shoreline position at each time.

linear extrapolation backwards in time is made to find the location of the base of this characteristic.

(*e*) The three Rankine–Hugoniot equations are solved simultaneously with the difference form of the Riemann equation (3.13) valid along the C^- characteristic arriving from the high side. This set of equations presents a system comprising four nonlinear equations in four unknowns and is solved numerically using a globally convergent Newton–Raphson technique (see Press *et al.* 2007).

(*f*) Values of the independent variables at the mesh point adjacent to the low side of the shock are computed by a linear interpolation between the low side of the shock (point L) and the next supercritical node.

(*g*) Values of the independent variables at the mesh point adjacent to the high side of the shock are computed by a linear interpolation between the high side of the shock (point H) and the next subcritical node.

B.4. *Type 2 (morphodynamic) shock*

(*a*) An initial estimate for the new shock location $\hat{x}_w$ at $n+1$ is made using the value of the shock speed at s. This is assumed to be known in the case of a pre-existing shock or is computed by the method given above for embedded shocks.

(*b*) Estimates of the C^+ and C_b wave speeds on the low side (at point L) and the C^- and C_b wave speeds on the high side (at point H) of the shock are made using values from the previous time step. The base points of these characteristics are found using linear extrapolation backwards in time.

(*c*) The three Rankine–Hugoniot equations are solved simultaneously with the two Riemann difference equations valid along the C^+ and C_b characteristics arriving from the low side and the two Riemann difference equations valid along the C^-

https://doi.org/10.1017/S0022112010002983 Published online by Cambridge University Press

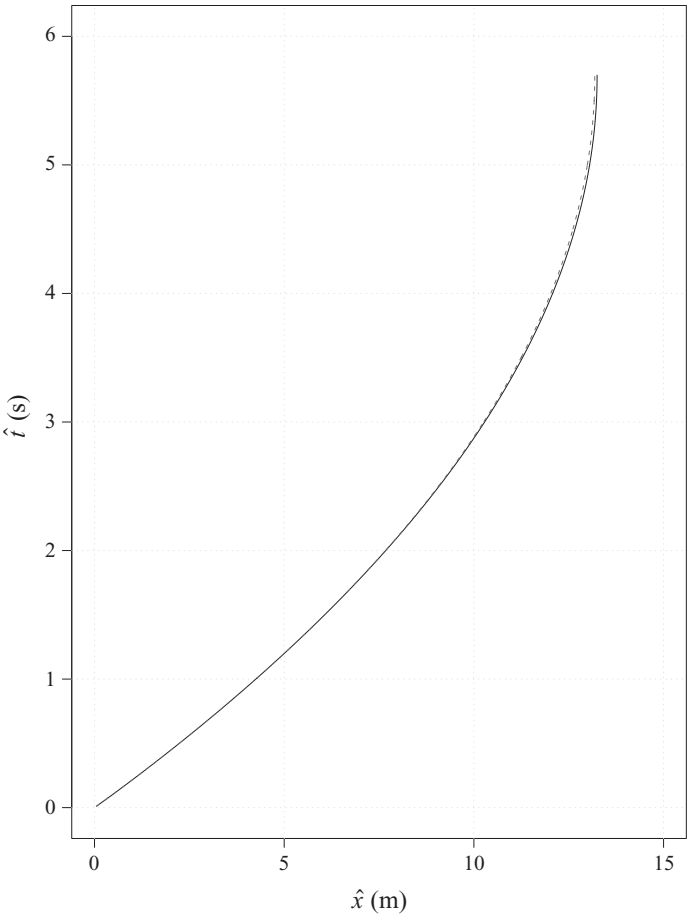


FIGURE 13. Comparison of the dimensional instantaneous shoreline position as computed by the STI MOC solver (solid line) and calculated from the numerical integration of (2.15) (dashed line) with $A = 4 \times 10^{-3}$ s^2 m^{-1} and $p = 0.4$.

and C_b characteristics arriving from the high side. This set of equations presents a system comprising seven nonlinear equations in seven unknowns and is again solved numerically using a globally convergent Newton–Raphson technique.

(*d*) Values of the independent variables at the mesh point adjacent to the low side of the shock are computed by a linear interpolation between the low side of the shock (point L) and the next supercritical node.

(*e*) Values of the independent variables at the mesh point adjacent to the high side of the shock are computed by a linear interpolation between the high side of the shock (point H) and the next subcritical node.

Note that the use of extrapolation or interpolation to compute values of dependent variables adjacent to shock points is standard practice when using the shock fitting approach. (Indeed, it is the only available option.) Consequently, there have been many in-depth studies undertaken into the effect of such procedures on the global accuracy of numerical solutions. We refer the interested reader to Moretti (2002) for an introduction to modern shock fitting techniques.

https://doi.org/10.1017/S0022112010002983 Published online by Cambridge University Press

Appendix C. Model verification

In order to verify our numerical model we check its ability to reproduce the analytical results presented in SM63. As the bed in the SM63 analytical solution is fixed, it is necessary to set the sediment mobility parameter equal to some small, but non-zero, value; here we use $A = 1 \times 10^{-10}$ s^2 m^{-1} and set beach porosity equal to zero. Figure 12 shows a comparison between the SM63 fixed-bed analytical solution and numerical 'fixed-bed' results for water depth and shoreline position. Results presented at the indicated times are dimensional; in this appendix carets have been dropped for convenience, and variables correspond to both the run-up and backwash. It is clear from the figure that the STI MOC scheme performs extremely well, with results being almost indistinguishable at this scale; in fact, for the time window shown, the relative error between numerical and analytical results is less than 0.5 %. A valuable check can be made on the accuracy of the numerical solution by comparing the instantaneous shoreline position predicted by the STI MOC scheme with that predicted by the numerical integration of (2.15). To integrate (2.15), a variable-time-step fourth-order Runge–Kutta scheme is used with the terms $\partial h/\partial x$ and $\partial b/\partial x$ approximated by simple backward differencing. The results of such an integration for a typical combination of A and p are shown in figure 13; clearly the agreement is excellent.

REFERENCES

Abramowitz, M. & Stegun, I. A. (Eds.) 1965 *Handbook of Mathematical Functions with Formulas, Graphs, and Mathematical Tables*. Dover.

Baldock, T. E., Kudo, A., Guard, P. A., Alsina, J. M. & Barnes, M. P. 2008 Lagrangian measurements and modelling of fluid advection in the inner surf and swash zones. *Coastal Engng* **55**, 791–799.

Barker, J. W. & Whitham, G. B. 1980 The similarity solution for a bore on a beach. *Commun. Pure Appl. Math.* **33**, 447–460.

Brocchini, M. & Baldock, T. E. 2008 Recent advances in modeling swash zone dynamics: influence of surf–swash interaction on nearshore hydrodynamics and morphodynamics. *Rev. Geophys.* **46**, 1–21.

Butt, T., Russell, P., Puleo, J., Miles, J. & Masselink, G. 2004 The influence of bore turbulence on sediment transport in swash and inner surf zones. *Cont. Shelf Res.* **24**, 757–771.

Carrier, G. F. & Greenspan, H. P. 1958 Water waves of finite amplitude on a sloping beach. *J. Fluid Mech.* **4**, 97–109.

Courant, R. & Friedrichs, K. O. 1976 *Supersonic Flow and Shock Waves*. Springer.

Dodd, N., Stoker, A. M., Garnier, R., Vittori, G., De Los Santos, F. J., Brocchini, M., Soldini, L. & Losada, M. 2008 Use of numerical models in determining the origin of beach morphology: a case study from La Barrosa beach, Spain. *Coastal Engng* **55** (7–8), 601–621.

Freeman, J. & Le Méhauté, B. 1964 Wave breakers on a beach and surges on a dry bed. *ASCE J. Hydraul. Div.* **90** (HY 2), 187–216.

Guard, P. A. & Baldock, T. E. 2007 The influence of seaward boundary conditions on swash zone hyrdodynamics. *Coastal Engng* **54**, 321–331.

Hibberd, S. & Peregrine, D. H. 1979 Surf and run-up on a beach: a uniform bore. *J. Fluid Mech.* **95**, 323–345.

Ho, D. V. & Meyer, R. E. 1962 Climb of a bore on a beach. Part 1. Uniform beach slope. *J. Fluid Mech.* **14**, 305–318.

Hsu, T.-J. & Raubenheimer, B. 2006 A numerical and field study on inner-surf and swash sediment transport. *Cont. Shelf Res.* **26**, 589–598.

Hudson, J. & Sweby, P. K. 2003 Formulations for numerically approximating hyperbolic systems governing sediment transport. *J. Sci. Comput.* **19**, 225–252.

Jeffrey, A. 1976 *Quasilinear Hyperbolic Systems and Waves*. Pitman.

https://doi.org/10.1017/S0022112010002983 Published online by Cambridge University Press

Keller, H. B., Levine, D. A. & Whitham, G. B. 1960 Motion of a bore over a sloping beach. *J. Fluid Mech.* **7** (2), 302–316.

Kelly, D. M. 2009 Bore-driven swash on a mobile beach. PhD thesis, School of Civil Engineering, University of Nottingham, Nottingham, UK.

Kelly, D. M. & Dodd, N. 2009 Floating grid characteristics method for unsteady flow over a mobile bed. *Comput. Fluids* **38**, 899–909.

Lai, C. 1986 Numerical modelling of unsteady open channel flow. In *Advances in Hydroscience*, vol. 14, pp. 95–121. Academic.

Masselink, G., Evans, D., Hughes, M. G. & Russell, P. 2005 Suspended sediment transport in the swash zone of a dissipative beach. *Mar. Geol.* **216**, 169–189.

Masselink, G. & Hughes, M. 1998 Field investigation of sediment transport in the swash zone. *Cont. Shelf Res.* **18**, 1179–1199.

Masselink, G. & Li, L. 2001 The role of swash infiltration in determining the beachface gradient: a numerical study. *Mar. Geol.* **176**, 139–156.

Masselink, G. & Puleo, J. A. 2006 Swash zone morphodynamics. *Cont. Shelf Res.* **26**, 661–680.

Mei, C. C. 1990 *The Applied Dynamics of Ocean Surface Waves*, 2nd edn., Advanced Series on Ocean Engineering, vol. 1. World Scientific.

Moretti, G. 1971 Complicated one-dimensional flows. *Tech. Rep.* Pibal 71-25. Department of Aerospace Engineering and Applied Mechanics, Polytechnic Institute of Brooklyn.

Moretti, G. 1973 Experiments in multi-dimensional floating shock-fitting. *Tech. Rep.* Pibal 73-18. Department of Aerospace Engineering and Applied Mechanics, Polytechnic Institute of Brooklyn.

Moretti, G. 2002 Thirty-six years of shock fitting. *Comput. Fluids* **31**, 719–723.

Moretti, G. & DiPiano, T. 1983 An improved lambda-scheme for one-dimensional flows. *Tech. Rep.* NASA contractor report 3712. NASA Langley Research Centre.

Needham, D. J. & Hey, R. D. 1991 On nonlinear simple waves in alluvial river flows: a theory for sediment bores. *Phil. Trans. R. Soc. Lond.* A **334**, 25–53.

Osborne, P. D. & Rooker, G. A. 1999 Sand re-suspension events in a high energy infragravity swash-zone. *J. Coastal Res.* **15**, 74–86.

Packwood, A. R. & Peregrine, D. H. 1980 The propagation of solitary waves and bores over a porous bed. *Coastal Engng* **3**, 221–242.

Peregrine, D. H. 1972 Equations for water waves and the approximations behind them. In *Waves on Beaches and Resulting Sediment Transport* (ed. R. E. Meyer), pp. 95–121. Academic.

Peregrine, D. H. & Williams, S. M. 2001 Swash overtopping a truncated beach. *J. Fluid Mech.* **440**, 391–399.

Press, W. H., Flannery, B. P., Teukolsky, S. A. & Vetterling, W. T. 2007 *Numerical Recipes: The Art of Scientific Computing*, 3rd edn. Cambridge University Press.

Pritchard, D., Guard, P. A. & Baldock, T. E. 2008 An analytical model for bore-driven run-up. *J. Fluid Mech.* **610**, 183–193.

Pritchard, D. & Hogg, A. J. 2005 On the transport of suspended sediment by a swash event on a plane beach. *Coastal Engng* **52**, 1–23.

Puleo, J. A., Butt, T. & Plant, N. G. 2005 Instantaneous energetics sediment transport model calibration. *Coastal Engng* **52**, 647–653.

Ritter, A. 1892 Die fortpflanzung der wasserwellen. *Ver. Dtsch. Ing. Z.* **36**, 947–954.

Sakkas, J. G. & Strelkoff, T. 1973 Dam-break flood in a prismatic dry channel. *ASCE J. Hydraul. Engng* **99**, 2195–2216.

Shen, M. C. & Meyer, R. E. 1963 Climb of a bore on a beach. Part 3. Run-up. *J. Fluid Mech.* **16**, 113–125.

Sieben, J. 1997 Modelling of hydraulics and morphology in mountain rivers. PhD thesis, School of Civil Engineering, Delft University of Technology.

Sieben, J. 1999 A theoretical analysis of discontinuous flow with a mobile bed. *J. Hydraul. Res.* **37** (2), 199–212.

Stoker, J. J. 1957 *Water Waves*. Interscience.

https://doi.org/10.1017/S0022112010002983 Published online by Cambridge University Press

Titov, V. V. & Synolakis, C. E. 1995 Modeling of breaking and nonbreaking long-wave evolution and run-up using VTCS-2. *ASCE J. Waterw. Port Coast. Ocean Engng* **121** (6), 308–316.

Watson, G., Peregrine, D. H. & Toro, E. 1992 Numerical solution of the shallow water equations on a beach using the weighted average flux method. In *Computational Fluid Dynamics* (ed. C. Hirsch), vol. 1. Elsevier.

Whitham, G. B. 1958 On the propagation of shock waves through regions of non-uniform area or flow. *J. Fluid Mech.* **4** (4), 337–360.

Wu, C. M. 1973 Unsteady flow in open channel with movable bed. In *International Symposium on River Mechanics*, Bangkok, Thailand.

https://doi.org/10.1017/S0022112010002983 Published online by Cambridge University Press